PERGAMON

Available online at www.sciencedirect.com
SCIENCE DIRECT®

Renewable and Sustainable Energy Reviews
7 (2003) 317–351

RENEWABLE & SUSTAINABLE ENERGY REVIEWS

www.elsevier.com/locate/rser

Solar transparent insulation materials: a review

N.D. Kaushika [a], K. Sumathy [b,*]

[a] *Centre for Energy Studies, Indian Institute of Technology, Hauz Khas, New Delhi, 110 016, India*
[b] *Department of Mechanical Engineering, University of Hong Kong, Pokfulam Road, Hong Kong*

Received 18 March 2003; accepted 1 May 2003

Abstract

This paper presents a status report on solar transparent insulation materials (TIM). It covers a survey of the literature, various physical and other properties of TIM devices, their classifications, applications, fabrication procedures, availability and cost trends. The global resurgence of research is clarified. Subsequently, the development of TIM cover systems (often referred to as advanced glazing) from such products as polymer sheets, capillaries and cellular profiles, is discussed. Their design and performance characteristics are investigated; results corresponding to experimental measurements, as well as computational models, are presented. An explicit comparative study of absorber parallel and absorber perpendicular configurations of TIM cover systems is presented. The TIM covers with black end cover plates, and cellular walls of high emissivity, as well as those with selective cover plates and cellular walls fully transparent to IR radiations, have relatively lower heat loss coefficients.

Keywords: Transparent insulation materials; Honeycomb; Thermal insulation; Advanced glazings; Solar thermal systems

Contents

* Corresponding author. Tel.: +852-2859-2632; fax: +852-2858-5415.
E-mail address: ksumathy@hkucc.hku.hk (K. Sumathy).

1364-0321/03/$ - see front matter
doi:10.1016/S1364-0321(03)00067-4

1. Introduction

Thermal insulation is the simplest means of preventing heat losses and achieving economy in energy usage. In industry, thermal insulation serves several important functions such as preventing heat leakage, saving energy, control of temperature and thermal energy storage. Conventional insulation materials are often opaque and porous, and can be classified into fibrous, cellular, granular and reflecting types [1]. The thermal characteristic of these insulation materials is specified in terms of thermal conductivity. Stagnant air is a good insulating material; it has a thermal conductivity of 0.026 W/m·K. Primitive people used the underlying principle of air insulation by lining their garments with fur to protect them from severe winter weather. Some commonly used thermal insulation materials, such as glass fibre (thermal conductivity: 0.0325), alumina silicate (0.035), mineral wool (0.0407) and calcium silicate (0.057) have low thermal conductivity, which depends on the number of air cells packed at the cores of solid media. The diameter of air cells is about 0.09 μm, which is smaller than the mean free path of air. Heat is transferred through the insulation by conduction in solid media, convection as well as radiation across air cells. There are always some losses from thermal energy systems insulated with opaque materials.

Transparent insulation materials (TIM) represent a new class of thermal insulation wherein air gaps and evacuated spaces are used to reduce the unwanted heat losses. It consists of a transparent cellular (honeycomb) array immersed in an air layer. The air layers are similar to conventional insulation materials with regard to the placement of air gaps in the transparent solid media. TIM are solar transparent, yet they provide good thermal insulation. They hold great promise for application in increasing the solar gain of outdoor thermal energy systems. Solar transmittance and heat loss coefficient are the two parameters used for their characterization. The fundamental physical principle used in TIM is the wavelength difference between solar radiation which is received by the absorber and IR radiation which is emitted by the absorber. This review presents a status report on TIM technology and applications.

Nomenclature

A	aspect ratio (L/d)
D	cell width of honeycomb (m)
E	fraction of cellular cross section area occupied by wall material
F	Hottel's shape factor for radiative exchange
F_{11}	geometrical shape factor for IR radiation with black end plates
G	acceleration due to gravity (m/s^2)
h_w	convective heat loss coefficient due to wind (W/m^2 K)
h_t	heat transfer coefficient from top surface of the MMA slab to the glass cover (W/m^2 K)
h_{pc}	combined conductive and radiative heat loss coefficient for the honeycomb cover system (W/m^2 K)
$I_b(t)$	solar beam radiation at time t (W/m^2)
$I_d(t)$	solar diffuse radiation at time t (W/m^2)
K	extinction coefficient of cover plate (m^{-1})
k	thermal conductivity of MMA slab (W/m^2 K)
k_s, k_a	scattering and absorption coefficient of CSD's wall material, respectively
L	depth of honeycomb (m)
N	number of cover plates
n	integer representing lowest rounded-off value of N
Q_L	total heat loss from the system (W/m^2)
Q_S	amount of solar radiation absorbed at the absorber plane (W/m^2)
Q_t	total heat loss from top surface (W/m^2)
Q_{t1}	heat loss from absorber plane to top cover (W/m^2)
Q_{t2}	heat loss form top cover to ambient (W/m^2)
$Q_U(t)$	retrieved heat flux per unit area of heater (W/m^2)
Ra	Rayleigh number
Ra_c	critical Rayleigh number for breakdown of the unstable region
R_θ	single surface reflectivity for the vertical wall of TIM
$S(t)$	solar intensity at time t (W/m^2)
T_c	top cover temperature of honeycomb array (°C)
T_p	absorber temperature (°C)
$T_a(t)$	ambient air temperature at time t (°C)
T_{sky}	sky temperature (°C)
T_g	glass cover temperature (°C)
U_1	heat loss coefficient from MMA slab top surface to ambient (W/m^2 K)
U_2	heat loss coefficient from glass cover to ambient (W/m^2 K)
U_L	overall heat loss coefficient (W/m^2 K)
V	wind speed (m/s)
x	coordinate (m)

Greek letters

α	material thermal diffusivity
$\alpha(\theta)$	absorptivity of the top (blackened) surface
$(\alpha\tau)_{eff}$	effective absorptivity–transmissivity product
β	tilt angle of water heating system (deg)
δ	thickness of cellular array wall (mm)
ν	kinematic viscosity (m^2/s)
ρ	albedo of the ground
σ	Stefan-Boltzman constant
ϕ	azimuth angle (degrees)
θ	angle of incidence (degrees)
θ_r	angle of refraction (degrees)
θ_{eg}, θ_{es}	equivalent beam angle of ground and sky radiation, respectively (degrees)
μ	refractive index of MMA slab material
μ_g	refractive index of top glass cover
ε_c	emissivity of top cover
ε_p	emissivity of absorber plane
ρ^s_ϕ	specular reflectivity
$\rho^s_{\phi e}$	equivalent specular reflectivity
$\rho^d_{\phi e}$	equivalent diffuse reflectivity
$\tau_C(\theta)$	transmittance (specular as well as diffuse) through the cell to beam radiation incident at an angle θ and azimuth angle ϕ)
$\tau_D(\theta)$	cell transmittance corresponding to specular reflection and refraction through the cells of beam radiation with incident angle θ and azimuth angle ϕ)
$\tau_E(\theta)$	transmittance through TIM walls
τ_{bg}	beam radiation transmittance for glass cover
τ_{dg}	ground diffuse radiation transmittance for MMA slab
τ_{ds}	sky diffuse radiation transmittance for MMA slab
τ_{dgg}	ground diffuse radiation transmittance for glass cover
τ_{dsg}	sky diffuse radiation transmittance for glass cover

2. Historical background

In solar energy context, Veinberg and Veinberg [2] investigated the use of “deep narrow meshes” as solar transparent honeycomb insulation in solar absorbers. Later, Francia [3] demonstrated the effectiveness of these anti-radiating cells in medium to high temperature solar energy absorbers. Hollands [4] presented the theoretical performance characteristics of a cellular honeycomb as a convection suppression

device (CSD) placed between the absorber and the outer glass cover of the flat plate collector. Tabor [5] presented a concise picture of cellular (honeycomb) arrays, indicating that successful use of honeycomb insulation should wait for better materials and manufacturing techniques. Since that time, extensive experimental, as well as theoretical, researches on honeycomb devices for suppressing the natural convection have been carried out (e.g. see [6] for review).

At the outset, natural convection across an air layer confined between solar glazing and absorber plate in the collector was investigated. Horizontal as well as inclined layers were considered. Subsequently, the effect of cellular arrays on convection suppression was formulated in terms of the escalation in critical Rayleigh number [7–17]. It has been pointed out that the convective stability of the fluid (air) in the honeycomb cell depends on the value of critical Rayleigh number (Ra_c), which depends on the physical shape, aspect ratio ($A = L/d$) and thermo physical properties of the walls of the cell. The fluid-mechanical treatment of this type of problem for square cells has been given by Edward and Catton [7], among others, following which Ra_c may be expressed as:

$$Ra_c = \frac{(a_0^2 + 23.9)^3}{(a_0^2 + 7.97)} \tag{1}$$

where $a_0 = \pi m\ (5)^{0.5}$ A and $0.75 \leq m \leq 1$ the Rayleigh number is given by

$$Ra = \frac{g\beta \Delta T L^3}{\alpha\ \nu} \tag{2}$$

So, for convection suppression

$$(\Delta T)_{\max} = \frac{Ra_c \alpha \nu}{g\beta L^3} \tag{3}$$

The $(\Delta T)_{\max}$values of air layer as obtained from Eq. (3) by Sharma and Kaushika [18], shows that for a cell width of ≤12.5 mm, convection is suppressed for the range of temperatures between 50 and 100 °C.

Furthermore, Guthrie and Charters [19], and Kaushika et al. [20], have observed that in the case of an inclined solar absorber, the motion is essentially up-slope. It has, therefore, been argued that parallel slat arrays (Fig. 1a,b), are quite sufficient to suppress convection in practical situations. The resultant device would involve a simplified fabrication procedure and would result in less insulation reaching the absorber than the convectional three-dimensional honeycomb (Fig. 1c).

The honeycomb device has also been investigated in relation to total heat loss (convection, conduction and radiation) reduction characteristics in a flat plate collector. Lalude and Buchberg [21], determined optimum values of design parameters for opaque rectangular honeycombs, as well as the design for a honeycomb based, porous-bed solar air heater. The design of cylindrical glass honeycombs, which minimize the cost of energy collected, was investigated by Buchberg and Edward [13]. These authors used the independent mode analysis (IMA), which assumes additive modes of heat transfer across the honeycomb cellular array. Subsequently, it was

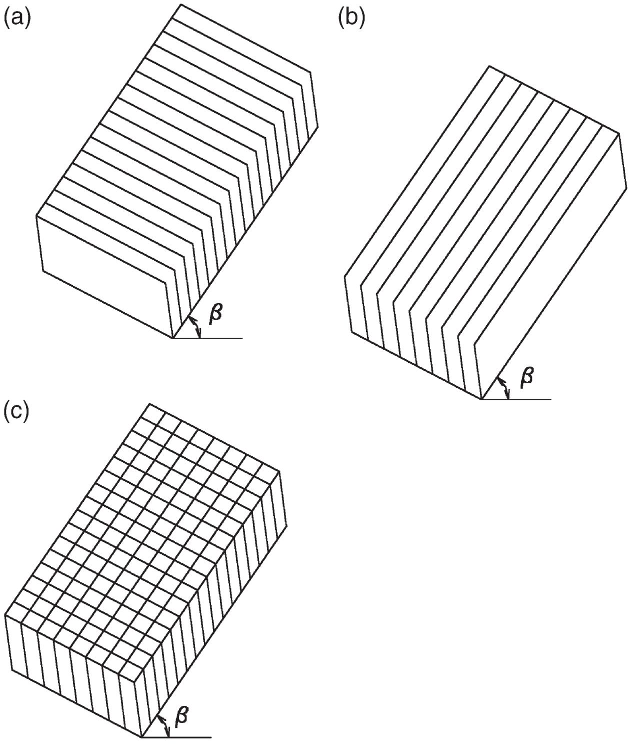


Fig. 1. Honeycomb and parallel slat arrays.

realized that IMA grossly underestimates the heat transport across a honeycomb; hence dependent mode analysis was developed to account for radiative–conductive coupling [22]. The performance of a flat-plate collector with a slatted convection-suppression device made of thin glass was studied experimentally by Charters and Guthrie [23]. Subsequent research involves an accurate determination of the solar transmittance, convective (for the critical and post critical Rayleigh regimes), and other thermal transfer characteristics of the device [18,19,24–29]. In practice, a flat plate collector with small-celled honeycomb and selective coating has been found to exhibit efficiency comparable to a vacuum tube collector (efficiency 50% at $\Delta T = 100$ K and solar irradiance of 800 W/m^2).

The honeycomb application as a convection suppression device in a solar flat plate collector did not prove very successful, because of the demanding characteristics of the materials and fabrication methods. Glass honeycomb devices were fragile and bulky for use in the solar collectors and the available plastics did not satisfy the stringent requirements for operating temperatures in excess of 80 °C. In the early eighties, a new concept was proposed for a non-convective solar pond using the honeycomb as transparent insulation. It was an attractive alternative to the salt gradient solar pond [27,30,31]. The simulation results of the honeycomb solar pond predicted solar collection efficiency up to 40–50% at 70–80 °C [18,32]. This has led

to extensive theoretical and experimental research on honeycomb devices such as TIM and their applications. In addition to the honeycomb solar collector, the transparent honeycomb insulated passive water heating system, using water as well as a ground (concrete/sand) as a collector/storage media has also been investigated [33–36]. The other applications of TIM include use in the solar passive heating of buildings [28,37–39], as a bifacial irradiated solar flat plate collector [40], a transparently insulated facade element for daylighting in office work space, solar cookers, solar storage ovens and solar hot air sterilizers. Some of these applications are schematically illustrated in Fig. 2. Several new configurations of TIM have been researched simultaneously. Optical transmittance and reflectance of several translucent samples over a solar wavelength range has been investigated [41] and many new plastics and manufacturing techniques have been tried. As frequently occurs with the resurgence of research on honeycomb insulation, alternative means were also explored. For example, transparent insulation characteristics of layers made of silica aero gel pellets [42] have been investigated. The pellets in diameters from 3 to 5 mm, were simply used to fill into the air gap. Progress in this area, along with progress in IR reflecting coatings, has led to a new branch of solar thermal technology, referred to as TIM. Six annual international workshops have been held; the proceedings of these workshops were published by Franklin Company, 192 Franklin Road, Birmingham B30 2HE UK. A special issue of Solar Energy vol. 45(5), 1992 also published a number of papers on the subject of TIM.

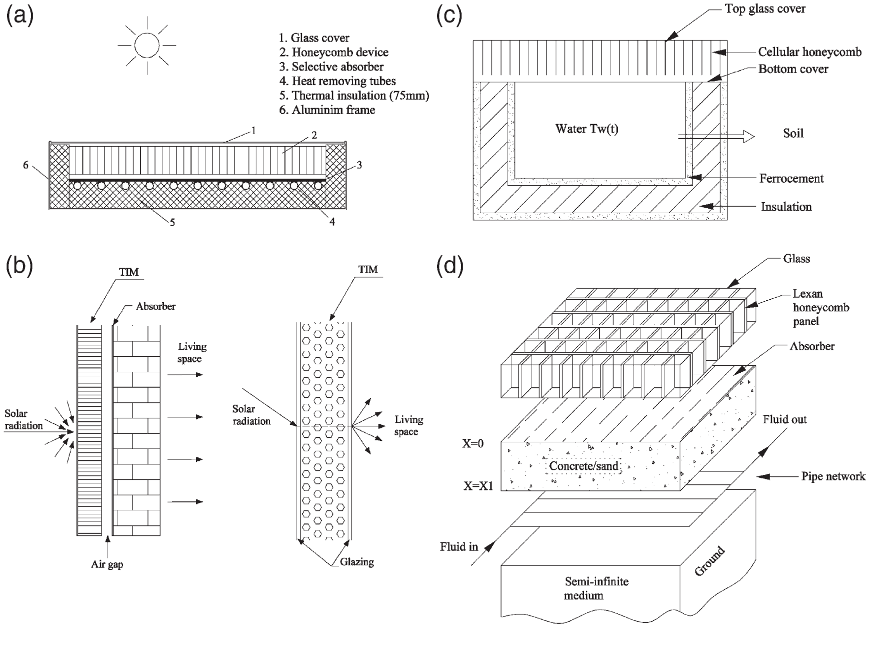


Fig. 2. a. Applications of TIM (a) solar collector (b) space heating (c) day lighting b. applications of TIM (a) saltless honeycomb solar pond (b) ground ICS system.

3. Classification

Several types of TIM are now recognized; they may be classified in accordance with various considerations, such as the manufacturing process, the material, and cellular geometry. The classification based on cellular geometry [43] is as follows:

1. Absorber-parallel
2. Absorber-perpendicular
3. Mixed configuration
4. Cavity structures
5. Homogeneous

These configurations are illustrated in Fig. 3. The absorber-parallel structures involve multiple covers of glass/plastic sheets, which are placed parallel to the absorber. The major problem associated with this structure is that the number of parallel covers must be increased to reduce heat loss, which reduces the solar transmittance and limits solar gain. In absorber perpendicular structures, cell walls are placed perpendicular to the absorber plane. The advantage of this configuration is the forward reflection of solar radiation by vertical walls, enabling a major portion of incident radiation to reach the absorber. The convection and radiation heat losses may be significantly suppressed by the proper design of the cell dimensions. The mixed and cavity structures are the combination of absorber-parallel and absorber-vertical structures; they include duct plates and multiple wall plastic sheets. The problem associated with this structure in lowered solar transmittance, but heat losses are also reduced significantly. Homogenous material includes the TIM of glass fibres and aero gels; these materials can be used for higher temperatures [44]. The heat transfer in aero gels consists of three components: solid conduction, pore gas conduction and irradiative heat transfers. The thermal conductivity of transparent silica aerogel increases sharply in the high temperature region. However, the increase is rather small for carbon opacified sample [45]. The radiation scattering and absorption are little more in these materials compared to other TIM.

The most documented configuration is the absorber perpendicular type, using honeycomb cellular arrays. Honeycomb cellular arrays have a long history in both natural and man made applications and some of these applications are listed in Table 1.

4. Fabrication of devices

Cobble [46] and Cobble et al. [47], suggested the use of a transparent slab of methyl methacrylate (MMA) as transparent insulation material use in a solar heat trap. Sheets of glass and polymer materials have also been used in multiple glazing. More recently, General Electric Plastic Industries, Ltd., has marketed multiwalled plastic sheets, which can also be used as absorber parallel TIM. Polygal Plastic Industries, Ltd., has marketed polycarbonate-structured sheet with spectral selectivity

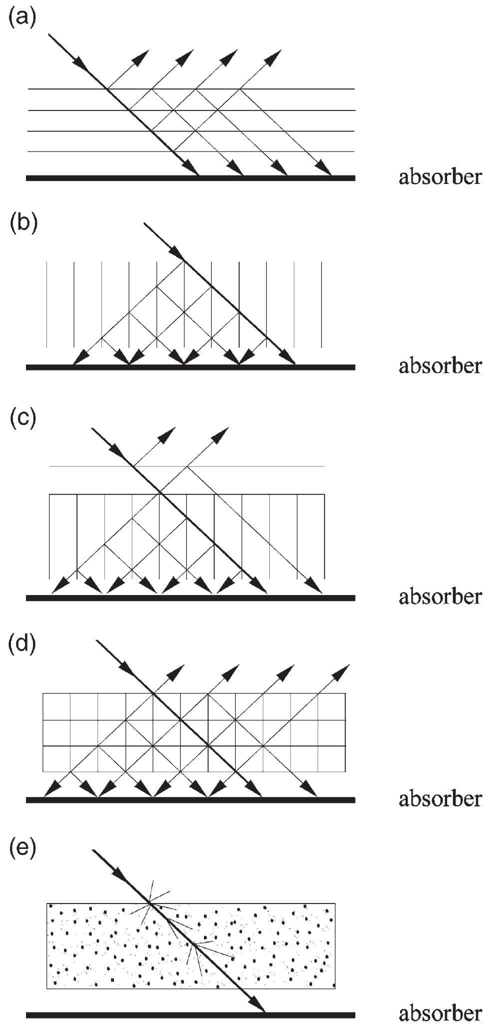


Fig. 3. Classification of transparent insulation materials.

[48]. Honeycombs of thick-walled glass material of 1–3 mm [3,13], non-transparent reflecting material [10], and thin-walled plastic-like polyester (FEP Teflon, polyethylene, acrylic etc.), have also been fabricated.

Engineers often cite the hexagonal shape of bee honeycomb as the most economical use of two-dimensional space. The hexagonal cross section was therefore, one of the earliest shapes to be considered; several cell shapes have subsequently been investigated. For example, among others, the hexagonal [49], square [11,24], rectangular [50,51], capillaries [25,52] and parallel slats [25,53] cross sections have been considered.

Fabrication of a thick-walled device is relatively simple [6]; the material chosen

Table 1
History of the applications of honeycomb devices

Millions of years ago	Bee’s honeycomb-like configuration existed in nature
2000 years ago	Paper honeycombs used by the Chinese for ornamental applications
1940	Hexagonal shape of bee honeycomb used by structural engineers as the most economic use of two-dimensional space. Modern honeycombs (metallic) used for: Strength in structural applications, Aircraft construction in aerospace industries
1960	Transparent honeycomb made of glass and polymer materials used as convection suppression device in solar flat plate collector
1980	The concept of transparent honeycomb insulated solar pond was advanced leading to extensive worldwide research on transparent-honeycomb insulation material (TIM) and applications in building and industries

for temperatures up to 70 °C could be poly methyl methacrylate (PMMA), often referred to as Perspex. Sheets of a thickness of 1 mm or less may be used. For the fabrication of honeycomb modules of the size (50 × 50 × 10 cm), the material is cut into slats of (50 × 10 cm). The slats are then interwoven to form a square cell of (1 × 1 cm). For the fabrication of thin-walled devices, the films of such materials as polycarbonate, polyester, FEP Teflon or fluorinated ethylene teraphithlate (FETP) could be used. Capillaries and profile extrusion products of various cross sections such as hexagonal, square and circle have been used to fabricate the cellular honeycomb arrays. However, the fabrication of devices from film material poses problems in glue dispensing. A relatively more expensive but technically convenient method of fabrication of square honeycomb has been devised and adopted by ArEl Energy Ltd., Israel; this method involves a profile extrusion process. The device is encapsulated in tempered glass, which protects the device from UV degradation (Fig. 4).

5. Cost trends

The major factor associated with the practical realization of the TIM insulated system is cost-effective manufacturing of the TIM device. During the last two decades, considerable progress has been made in this regard. The optical and thermal properties of several plastic materials have been surveyed. GE Plastics has recently begun the commercial manufacturing of structured products of lexan material (polycarbonate material). Some of these products are transparent and can be used as cavity type TIM. The cost in India is quoted as US\$360–400/m^2.

The cost of TIM manufactured by ArEl Energy Ltd., Israel, was quoted at US\$100/m^2 in 1990. Recently, Schaefer and Lowrey [32] gave the cost of optimized honeycomb covers made of Mylar and Lexan as \$9/m^2 and \$7/m^2, respectively. In 1976, a Tedlar device with dimensions of 0.03 mm (δ) thick, $(\alpha\tau)_{\mathrm{eff}}$ of 0.72 and aspect ratio of 5 ($A = L/d$) cost US\$19/m^2. Hollands et al. [54] proposed an industrial manufacturing technique for the honeycomb device.

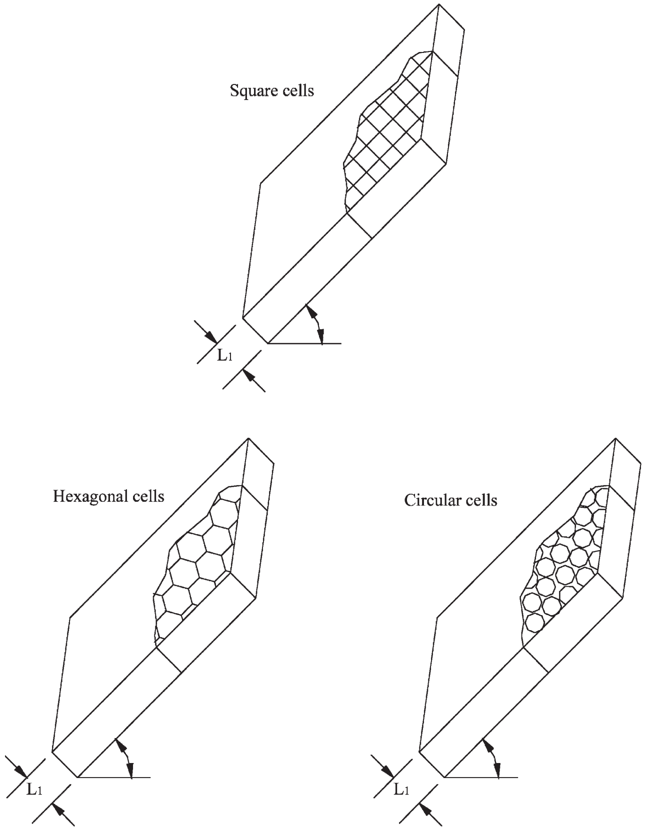


Fig. 4. Encapsulated TIM cover systems.

The costs of TIM noted above are approximate, owing to rather inconsistent quotations from the manufacturers, who are still in the experimental phase.

6. Characterization of devices

The intended objective for the TIM device is to maximize solar heat collection across the device; this involves the consideration of solar radiation transmittance and heat transfer mechanisms across the device. The data related to solar transmittance and the heat loss coefficient are now available from assorted experimental measurements and test values, as well as from computational models. Following is the data and models which are intended to be helpful for engineering design, as well as for trade-off strategies required to establish a balance between many constraining factors related to the cost of the TIM device.

6.1. Experimental measurements

Symons et al. [55] and Symons [25] used an integrating sphere (Fig. 5) with a large sample port and a collimated beam for solar transmittance measurements of planar, as well as cellular (honeycomb) samples. The measurements covered a range of cellular samples of incidence angles between 0° and 60°. Thin-walled cellular samples of small aspect ratio, cell length (L), divided by the hydraulic cell diameter (d), were considered. They reported good agreement of measurements with the simple model used by Hollands et al. [24]. Subsequently, Platzer [51,52] used the integrating sphere technique for measurements of solar transmittance of cellular (honeycomb) samples covering a wider range of aspect ratio and incidence angle. He suggested the fitting functions for measured data as follows:

$$\tau(\theta) = \tau_0 \exp(-a \cdot \tan\theta) \quad (4)$$

$$\tau_0(L) = \tau_{00} + \tau_{01}L \quad (5)$$

$$a(L) = a_0 + a_1 L \quad (6)$$

where L is depth of cell, honeycomb thickness, and 'a' is the effective absorption parameter, which is proportional to the aspect ratio of samples. The values of the above mentioned constants for sample cellular materials are summarized in Table 2.

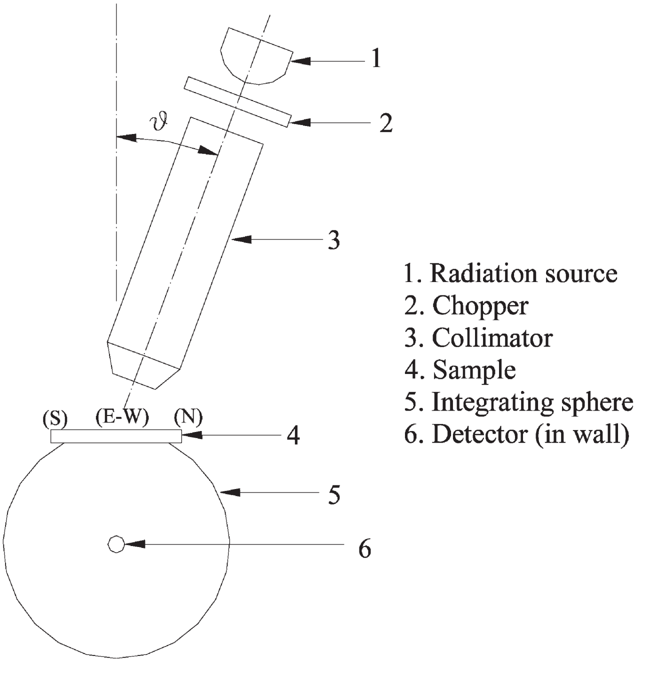


Fig. 5. Integrating sphere apparatus for measuring solar transmittance.

Table 2
Coefficients for calculating solar transmittance dependent on incidence angle and material thickness [52]

No	Plastic type	τ_{00}	τ_{01} (cm^{-1})	a_0	a_1 (cm^{-1})
1	Polymethylmethacrylate	0.936	−0.0144	0.0934	0.0089
2	Polycarbonate	0.795	0.0000	0.0444	0.0222
3	Polytetrafluorethylene-derivative	0.932	−0.0266	0.1220	0.2050
4	Polymethylmethacrylate	0.900	0.0000	0.0944	0.0085
5	Polycarbonate	0.970	−0.0040	0.0140	0.0144
6	Polycarbonate	0.970	−0.0040	0.0100	0.0143

Heat is transferred through the cellular (honeycomb) device by one or more of the following modes:

– conduction and radiation through the solid cellular walls
– conduction, convection and radiation across the air cell.

The total heat transport across the honeycomb device is mainly due to conduction and radiation, as the convection is usually suppressed. Measurements of heat transfer across TIM devices have been carried out using the hot plate apparatus [56], wherein the hot plate is electrically heated to 200 °C (T_h) and the cold plate is thermostatically controlled at a desired temperature (T_c). The sample is placed between the plates. The quantity measured is effective heat conductance (defined as the effective heat loss coefficient, W/m^2 K), heat flux through the sample divided by ($T_h - T_c$). The dependence of these values on the thickness of the TIM device is shown in Table 3 [56]. With a view to investigating the high temperature (>80 °C) performance of the honeycomb solar collector, the measurements of stagnation temperature have also been carried out by some authors [57]. In these experiments, it was observed that the small-celled polycarbonate honeycomb started melting at 120 °C; with the introduction of an air gap between the absorber and the honeycomb device, the highest allowable temperature is estimated to be 140 °C. From the consideration of solar transmittance and U_L values of the small-celled TIM device, the stagnation temperature of a TIM solar collector is estimated as 250 °C.

Table 3
Effect of the thickness of small-celled honeycomb TIM device on total heat conductance [56]

Thickness L (m)	Heat conductance (W/m^2 K)
0.02	3.5
0.04	2.1
0.06	1.6
0.08	1.3
0.10	1.1

6.2. Computational models

The above mentioned experimental measurements correspond to different cellular devices, which are either commercial, or have been produced by the same organizations for test purposes. Most of the cellular devices tested to date are made of plastic. Seldom, if ever, have glass honeycomb materials been included. These few samples may not be considered representative of future products. Furthermore, even for the available honeycomb materials, a consistent set of solar transmittance and heat loss data, as functions of temperature (ΔT) and aspect ratio, is not available to enable for optimization of a specific system. Therefore, in the following section the modeling approach for investigating the design and performance characteristics of TIM cover systems is presented.

6.2.1. Absorber-parallel configuration

The absorber parallel configuration is very simple for practical realization and has been thoroughly researched for its solar heat trap characteristics. For example, a transparent slab of methyl methacrylate was suggested and tested by Cobble [46] and Cobble et al. [47], for the solar heat trap. The concept has since been subjected to theoretical [58–61] and experimental [62] investigations for various applications such as passive solar buildings, flat-plate collectors and integrated collector storage systems. All these analyses have involved several approximations, such as (i) the solar transmittance of MMA slabs, corresponding to diffuse components of solar radiation is not taken into account, (ii) the beam radiation transmittance is considered only at normal incidence. Furthermore, some of the above mentioned analyses have used incorrect boundary conditions for heat transfer at the top surface of the MMA slab [63]. The resulting predictions are therefore of doubtful merit. In recent work [6,64], an improved analysis of solar thermal processes is carried out to evaluate the transparent insulation characteristics of a TIM slab placed on the absorber plane with and without glass cover, as shown in Fig. 6a,b, respectively. The solar radiation incident on the top of the slab is partly reflected and partly absorbed; the remainder is transmitted to the absorber plane, where complete absorption takes place. The distributed heat generation in the slab guards the absorber and traps the heat. The following assumptions are made in modeling the solar thermal processes:

(a) sky and ground diffuse radiation is isotropic;
(b) emission of radiation within the slab due to internal heat generation is ignored;
(c) absorber plane is in direct contact with the slab, so there is no discontinuity in temperature at the interface;
(d) conductive heat transfer inside the slab is one dimensional.

Solar radiation flux ($I(x)$), available at any distance x, is given by

$$I(x) = I_b R_b \tau_{bg} \tau_b(x) + I_d R_d \tau_{dsg} \tau_{ds}(x) + (I_b + I_d) R_l \tau_{dgg} \tau_{dg}(x) \quad (7)$$

For configuration without a glass cover, τ_{bg}, τ_{deg} and τ_{dgg} are equal to unity. The beam radiation transmittance for the thickness x of the slab, $\tau_b(x)$ is

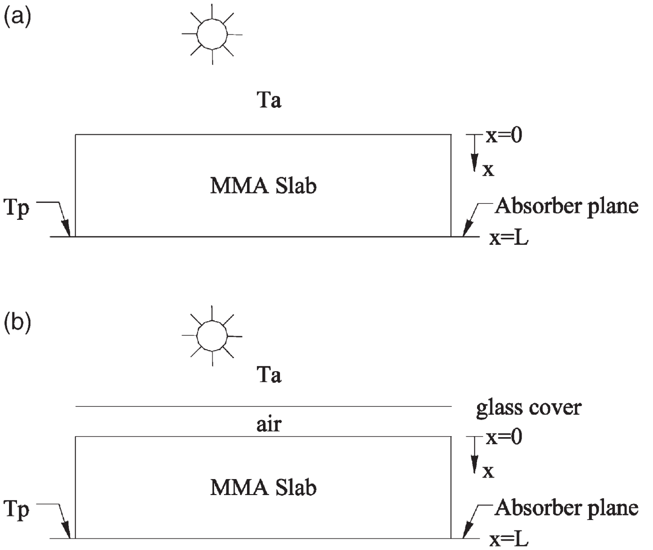


Fig. 6. Schematic view of the TIM slab on the absorber plane (a) without glass cover (b) with glass cover.

$$\tau_b(x) = \frac{1}{2}\tau_a(x)\left[\frac{(1-\rho_1)^2}{(1-\rho_1^2\tau_a^2(x))} + \frac{(1-\rho_2)^2}{(1-\rho_2^2\tau_a^2(x))}\right] \quad (8)$$

where

$$\rho_1 = \sin^2(\theta_r-\theta)/\sin^2(\theta_r+\theta)$$

$$\rho_2 = \tan^2(\theta_r-\theta)/\tan^2(\theta_r+\theta)$$

and $\mu = \sin(\theta)/\sin(\theta_r)$. For normal incidence $\theta = 0$, and $\rho_1 = \rho_2 = (1-\mu)^2/(1+\mu)^2$. The transmittance based on absorption, $\tau_a(x)$ is given by Cobble et al. [47]:

$$\tau_a(x) = \sum_{i=1}^{n} W_i e^{\frac{-\mu_i x}{\cos(\theta_r)}} \quad (9)$$

The values of n, W_i and μ_i are the parameter characteristics of solar transmission in the material. For an MMA slab, the values are as follows:

$W_1 = 0.081373;\ \mu_1 = \infty$

$W_2 = 0.668800;\ \mu_2 = 2.378$

$W_3 = 0.086103;\ \mu_3 = 12.55$

$W_4 = 0.061200;\ \mu_4 = 31.0$

$W_5 = 0.102400;\ \mu_5 = \infty$

The sky diffuse radiation transmittance $\tau_{ds}(x)$, and ground diffuse radiation transmit-

tance $\tau_{dg}(x)$ for the slab thickness with absorber plane tilt angle β, are given by [65,66]:

$$\tau_{ds}(x) = \frac{\int_0^{\frac{\pi}{2}-\beta}\int_{-\frac{\pi}{2}}^{\frac{\pi}{2}}\tau_b(x)\cos\theta\sin\theta\,d\phi\,d\theta + \int_{\frac{\pi}{2}-\beta}^{\frac{\pi}{2}}\int_{-\frac{\pi}{2}}^{\sin^{-1}\left(\frac{\cos\beta}{\tan\theta}\right)}\tau_b(x)\cos\theta\sin\theta\,d\phi\,d\theta}{\int_0^{\frac{\pi}{2}-\beta}\int_{-\frac{\pi}{2}}^{\frac{\pi}{2}}\cos\theta\sin\theta\,d\phi\,d\theta + \int_{\frac{\pi}{2}-\beta}^{\frac{\pi}{2}}\int_{-\frac{\pi}{2}}^{\sin^{-1}\left(\frac{\cos\beta}{\tan\theta}\right)}\cos\theta\sin\theta\,d\phi\,d\theta} \tag{10}$$

$$\tau_{dg}(x) = \frac{\int_{-\frac{\pi}{2}}^{\frac{\pi}{2}}\int_{\sin^{-1}\left(\frac{\cos\beta}{\tan\theta}\right)}^{\frac{\pi}{2}}\tau_b(x)\cos\theta\sin\theta\,d\phi\,d\theta}{\int_{\frac{\pi}{2}-\beta}^{\frac{\pi}{2}}\int_{\sin^{-1}\left(\frac{\cos\beta}{\tan\theta}\right)}^{\frac{\pi}{2}}\cos\theta\sin\theta\,d\phi\,d\theta} \tag{11}$$

The temperature distribution in the slab is given by the following equations: Configuration without glass cover,

$$k\frac{d^2T}{d^2x} - \frac{dI(x)}{dx} = 0, \tag{12}$$

where the boundary conditions are

$$\text{at} \quad x = 0 \quad -k\frac{dT}{dx} = -U_l(T|_{x=0} - T_a)$$

$$\text{at} \quad x = L \quad T|_{x=L} = T_p$$

Configuration with glass cover,

$$k\frac{d^2T}{d^2x} - \frac{dI(x)}{dx} = 0, \tag{13}$$

where the boundary conditions are

$$\text{at} \quad x = 0 \quad -k\frac{dT}{dx} = -h_t(T|_{x=0} - T_g)$$

$$\text{at} \quad x = L \quad T|_{x=L} = T_p$$

The energy balance equation for the glass cover is given as:

$$h_t(T|_{x=0} - T_g) = U_2(T_g - T_a) \tag{14}$$

The net energy balance equation for the glass cover is

$$Q_{net} = I(L) - k\left.\frac{dT}{dx}\right|_{x=L} \tag{15}$$

and the average efficiency is given as:

$$\eta = \frac{Q_{\mathrm{net}}}{S} \tag{16}$$

The term $k\left.\frac{\mathrm{d}T}{\mathrm{d}x}\right|_{x=L}$ for the two cover systems may be obtained by solving the one dimensional heat conduction Eqs. (12) and (13) with their respective boundary conditions, and may be expressed as follows:
Configuration without glass cover

$$k\left.\frac{\mathrm{d}T}{\mathrm{d}x}\right|_{x=L} = I(L)-I(0) + U_1(T_\mathrm{c}-T_\mathrm{a}) \tag{17}$$

Configuration with glass cover

$$k\left.\frac{\mathrm{d}T}{\mathrm{d}x}\right|_{x=L} = I(L)-I(0) + U_2(T_\mathrm{g}-T_\mathrm{a}) \tag{18}$$

6.2.2. Absorber-perpendicular configuration

The solar transmittance and heat loss reduction characteristics of cellular arrays have been extensively investigated during the last two decades. The absorber-perpendicular cover system consists of a cellular (honeycomb or capillary) array immersed in an air layer. It is generally encapsulated to protect against weathering and dust (Fig. 4). The glazings made from TIM are often referred to as advanced glazings. The solar radiation propagation through such a glazing is characterized by the transmittance–absorptance product, which is an essential input for studying the performance of the TIM based systems [26]. The transmittance–absorption product corresponding to beam and diffuse radiation, for three practical cases: (i) cellular matrix, (ii) cellular matrix with top encapsulation and (iii) cellular matrix with top and bottom encapsulation, has been investigated by Kaushika and Arulanantham [67].

The schematic diagram of a honeycomb cover system is as shown in Fig. 7. The

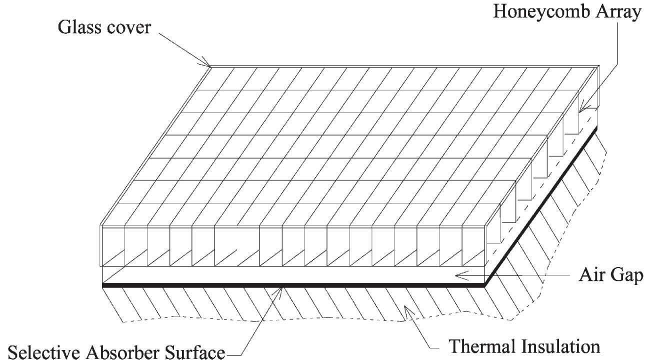


Fig. 7. Schematic view of honeycomb with air gap and glass cover.

honeycomb is placed on the absorber plane with a small gap, and its top is encapsulated with a glass cover of 3 mm thickness with low extinction coefficient (5 m^{-1}), which corresponds to the characteristics of tempered glass. The air layer and cellular array are considered to be in the non-convective state of air media. Since the main aim of the study is to characterize the honeycomb cover system, it is assumed that the sides and bottom of the absorber plane are perfectly insulated in such a way that there is no heat loss. The steady state energy balance for the absorber plane may be expressed as:

$$Q_U = Q_S - Q_L \tag{19}$$

The amount of solar radiation which is absorbed by the horizontal plane of the absorber, Q_s is

$$Q_S = I_b(\tau\alpha)_b + I_d(\tau\alpha)_s \tag{20}$$

The total heat loss through the cover system, Q_L, is calculated by the following method:
The heat loss from the absorber plane to the top glass cover is

$$Q_{t1} = h_{pc}(T_p - T_g) \tag{21}$$

where h_{pc} is the combined conductive and radiative heat loss coefficient for the honeycomb cover system. Arulanlantham and Kaushika [68] have examined the coupled conductive and radiative heat transfer for the determination of h_{pc} in detail. The computer program based on the procedure adopted by these investigators was made available for further computations. The heat loss from top glass cover to ambient, Q_{t2} consists of the convective and radiative components and may be expressed as [69]:

$$Q_{t2} = Q_{t2c} + Q_{t2r} \tag{22}$$

$$Q_{t2} = h_w(T_p - T_a) + \sigma\varepsilon_c(T_g^4 - T_{sky}^4) \tag{23}$$

where h_w, the convective heat transfer coefficient from top cover to ambient is given by [69]:

$$h_w = 5.7 + 3.8\ \mathrm{V} \tag{24}$$

In the steady state $Q_t = Q_{t1} = Q_{t2}$, so the value of T_c may be obtained by iterating Eqs. (22) and (23), so that $Q_{t1} = Q_{t2}$, using the Secant iteration method [70] to an accuracy of 0.001. The overall heat loss coefficient U_L, is obtained as:

$$U_L = \frac{Q_L}{T_p - T_a} \tag{25}$$

The efficiency of the compound honeycomb surface insulation may be expressed as:

$$\eta = \frac{Q_S - Q_L}{S(t)} \tag{26}$$

or

$$\eta = (\alpha\,\tau)_{\mathrm{eff}} - \frac{Q_{\mathrm{L}}}{S(t)} \tag{27}$$

The transmittance–absorption products $(\tau\alpha)_{\mathrm{b}}$ and $(\tau\alpha)_{\mathrm{s}}$ of a honeycomb cover system for solar beam and diffuse radiations are essential inputs for the determination of Q_{s}. The $(\tau\alpha)_{\mathrm{b}}$ may be expressed by an approximate equation, which does not take into account the internal reflections between the honeycomb and the cover, as follows:

$$(\tau\alpha)_{\mathrm{b}}(\theta) = \tau_1(\theta)\cdot\tau_2(\theta)\cdot\tau_3(\theta)\cdot\alpha(\theta) \tag{28}$$

$$\tau_N(\theta) = \tau_1(\theta)\cdot\tau_2(\theta) \tag{29}$$

where $\tau_1(\theta)$ is the transmittance based on reflection of the encapsulating cover plates, and is given by following [69]:

$$\tau_1(\theta) = \frac{1}{2}\left[\frac{1-\rho_{\mathrm{I}}}{1+(2N-1)\rho_{\mathrm{I}}} + \frac{1-\rho_{\mathrm{II}}}{1+(2N-1)\rho_{\mathrm{II}}}\right] \tag{30}$$

where

$$\rho_{\mathrm{I}} = \frac{\sin^2(\theta_{\mathrm{r}}-\theta)}{\sin^2(\theta_{\mathrm{r}}+\theta)} \qquad \rho_{\mathrm{II}} = \frac{\tan^2(\theta_{\mathrm{r}}-\theta)}{\tan^2(\theta_r+\theta)}$$

with

$$\frac{\sin\theta}{\sin\theta_{\mathrm{r}}} = \mu_{\mathrm{g}}, \quad \text{when} \quad \theta = 0$$

$$\rho_{\mathrm{I}} = \rho_{\mathrm{II}} = \frac{(1-\mu_{\mathrm{g}})^2}{(1+\mu_{\mathrm{g}})^2}$$

$\tau_2(\theta)$ is the transmittance based on absorption of the encapsulating cover plate and is given by Bougers law,

$$\tau_2(\theta) = \mathrm{e}\left(\frac{NK\delta_1}{\cos\theta_{\mathrm{r}}}\right) \tag{31}$$

where N is the number of encapsulating covers, K is the extinction coefficient and δ_1 is the thickness of the covers.

Studies for the determination of solar beam radiation transmittance of cellular array have been carried out by several authors, including Feland and Edwards [71], Hollands et al. [24], Symons [25], Platzer [72], Kaushika and Padmapriya [53] and Platzer [51,52]. Methods such as the Monte-Carlo techniques and the analytical approach have been used. Among others, square cell cross- sections have been considered [24,25,52,72,73].

Following Hollands et al. [24], Kaushika and Padmapriya [53] and Arulanantham and Kaushika [66], the beam radiation transmittance of cellular array for square cells, $\tau_3(\theta)$ may be expressed as:

$$\tau_3(\theta) = \frac{\tau_{\mathrm{C}}(\theta) + \tau_{\mathrm{E}}(\theta)\cdot E}{1-E} \tag{32}$$

where E is a fraction of the cellular cross-section area, occupied by wall material, having a square cell, and expressed as:

$$E = \frac{\delta\,(\delta + 2d)}{d^2} \tag{33}$$

$\tau_C(\theta)$ is the beam radiation transmittance through cell wall material having perfectly equivalent diffuse ($\rho^d_{\phi e}$), specular ($\rho^s_{\phi e}$) and absorptivity $\alpha(\phi)$.

$$\tau_C(\theta) = \tau_D(\theta) + \frac{\rho^d_{\phi e}}{\rho^d_{\phi e} + \alpha(\phi)}\cdot F_{11}[1-\tau_D(\theta)] \tag{34}$$

$$\tau_D(\theta) = (\rho^s_{\phi})^n(n + 1-N) + (\rho^s_{\phi})^{n+1}(N-n) \tag{35}$$

The absorptivity of the cell wall may be given as ($0 < \phi < 90$):

$$\alpha(\phi) = 1-\rho^d_{\phi e}-\rho^s_{\phi e} \tag{36}$$

where N is the number of walls intercepted by the solar ray in its propagation through cellular arrays, and 'n' is the lower rounded off value of N. For incoming solar radiation at incidence angle θ, N may be expressed for square cells as:

$$N = \frac{L}{d}\tan\theta \tag{37}$$

and

$$\phi = \frac{\pi}{2}-\theta \tag{38}$$

The above expression for N is an approximate form attributable to Symons [25] and Platzer [51]. The transmittance through the cell wall $\tau_E(\theta)$ may be expressed as:

$$\tau_E(\theta) = (1-R_\theta)^2\cdot e^{-b_\theta} + F\cdot\left(\frac{k_s}{k_s + k_a}\right)\cdot(1-e^{-b_\theta})\cdot(1-R_\theta) \tag{39}$$

where

$$b_\theta = \frac{(k_s + k_a)\cdot\mu\cdot L}{(\mu^2-\sin^2\theta)^{1/2}} \tag{40}$$

and

$$\frac{k_s}{k_s + k_a} = \frac{\rho^d_{\phi e}}{\rho^d_{\phi e} + \alpha(\phi)} \quad (\text{at } \phi = 0) \tag{41}$$

and

$$R(\theta) = \frac{1}{2}\left[\frac{\tan^2(\theta-\theta_r)}{\tan^2(\theta + \theta_r)} + \frac{\sin^2(\theta-\theta_r)}{\sin^2(\theta + \theta_r)}\right] \tag{42}$$

Similarly, $R(\phi)$ at angle ϕ is expressed as:

$$R(\phi) = \frac{1}{2}\left[\frac{\tan^2(\phi-\phi_r)}{\tan^2(\phi+\phi_r)} + \frac{\sin^2(\phi-\phi_r)}{\sin^2(\phi+\phi_r)}\right] \tag{43}$$

where $\phi_r = \sin\phi/\mu$ at angle ϕ. Equivalent specular reflectivity at $0 < \phi < 90$

$$\rho^{s}_{\phi e} = R(\phi) + \frac{(1-R(\phi))\cdot\alpha(\phi)}{1-R(\phi)\cdot\alpha(\phi)} \tag{44}$$

At an angle ϕ

$$\alpha(\phi) = \exp\left[\frac{-\mu(k_s-k_a)\cdot\delta}{(\mu^2-\sin^2\phi)^{1/2}}\right] \tag{45}$$

and at angle $\phi = 0$ is given by

$$\alpha(\phi = 0) = \frac{\rho^{s}_{\phi e}(\phi = 0)-R}{1-2R + R\rho^{s}_{\phi e}(\phi = 0)} \tag{46}$$

and

$$k_s + k_a = \frac{-\ln\alpha(\phi = 0)}{\delta}x \tag{47}$$

Thus, the absorptivity of the cell wall at angle ϕ is given by

$$\alpha(\phi) = 1-\rho^{d}_{\phi e}-\rho^{s}_{\phi e} \tag{48}$$

Transmittance of honeycomb array for diffuse radiation can be obtained by integration of beam radiation results over an appropriate range of incidence angles. Solar diffuse radiation transmittance for the plane glass cover of a flat plate collector has been investigated by Brandemuehl and Beckman [65]. Using the same approach, solar diffuse radiation transmittance for honeycomb array has been investigated by Arulanantham and Kaushika [66]. In the above investigation, the formulations take into account reflection, scattering and absorption by cell walls. A numerical integration technique is employed and results are converted in terms of equivalent beam angle of incidence; its variations as functions of tilt angle and aspect ratio for the lexan square celled honeycomb are given by polynomial equations as follows:
Ground radiation

$$\theta_{eg} = 90-0.60845\beta + 3.7097 \times 10^{-4}\beta A-3.0577 \times 10^{-5}\beta A^2 + 3.0328 \times 10^{-3}\beta^2-5.0287 \times 10^{-5}\beta^2 A + 4.157 \times 10^{-7}\beta^2 A^2 \tag{49}$$

Sky radiation

$$\theta_{es} = 59.69678-0.380354A + 4.2715 \times 10^{-3}A^2-0.1429\beta -8.055 \times 10^{-3}A\beta + 2.1229 \times 10^{-4}A^2\beta + 1.5277 \times 10^{-3}\beta^2 + 7.0696 \times 10^{-3}A\beta^2-2.1496 \times 10^{-6}A^2\beta^2 \tag{50}$$

The above formulations may be used to investigate the heat loss reduction and

solar energy gain characteristics of the TIM cover systems as functions of geometrical and operational parameters. The configurations comprising cellular array, as well as with top and bottom encapsulations, are considered. The cellular array concerns a commercially available honeycomb material of polycarbonate, which has a rectangular cross section of approximately 4.5 mm by 3.8 mm with a mean wall thickness of about 60 μm. Other thermophysical parameters used in the calculations are as follows:

$V - 3.0$ m/s

$T_a = 293$ K

$I_b = 500$ W/m^2

$\delta = 60$ μm

$\varepsilon_p = 0.9$ (for black absorber)

$\varepsilon_c = 0.9$

$I_d = 236$ W/m^2

The variations of effective transmittance–absorption products $(\alpha\tau)_{\rm eff}$, solar collection efficiency (η) and heat loss coefficient ($U_{\rm L}$) of cellular honeycomb panels with cell dimensions (i.e. d and L) at different angles of incidence 10°, 40° and 70°, for black and selective absorbers at a fixed absorber temperature of 70 °C, are shown in Figs. 8–11. The effect of air gap on heat transfer mode coupling analysis is made apparent. The coupling of radiation and conduction modes, due to absorbing emitting walls of honeycomb, tends to reduce the effect of selective coating. With the introduction of an unbound air layer of about 10 mm thickness between the absorber and honeycomb panel, conductive decoupling takes place and performance improves in both black and selective absorbers. The bounding cover plates of encapsulation tend to reduce the total heat loss coefficient; this is illustrated in Tables 4 and 5. It is seen that the following TIM cover systems have lowest heat loss coefficients: TIM covers with black end plates and cellular walls of high emissivity; TIM covers with selective end plates and cellular walls fully transparent to IR radiation. The reduction in transmittance due to the two covers is about 12% and 17%, respectively. It is therefore desirable to have covers of high quality glass with low iron content.

6.2.3. *Comparative study*

Comparison of the thermal performance of the absorber-parallel and absorber-perpendicular cover systems is illustrated and Table 6. The MMA slab system has an efficiency lower of about 12% than the honeycomb cover system. However, the slab system shows higher efficiencies compared to single and double glass cover. Reddy and Kaushika [74] have theoretically and experimentally investigated the performance of transparently insulated integrated-collector-storage (ICS) solar water heaters for a comparative study of cover systems having TIM devices placed between top glazing and the absorber. The resulting data on solar transmittance and heat loss coefficients of various TIM cover systems is illustrated in Table 7.

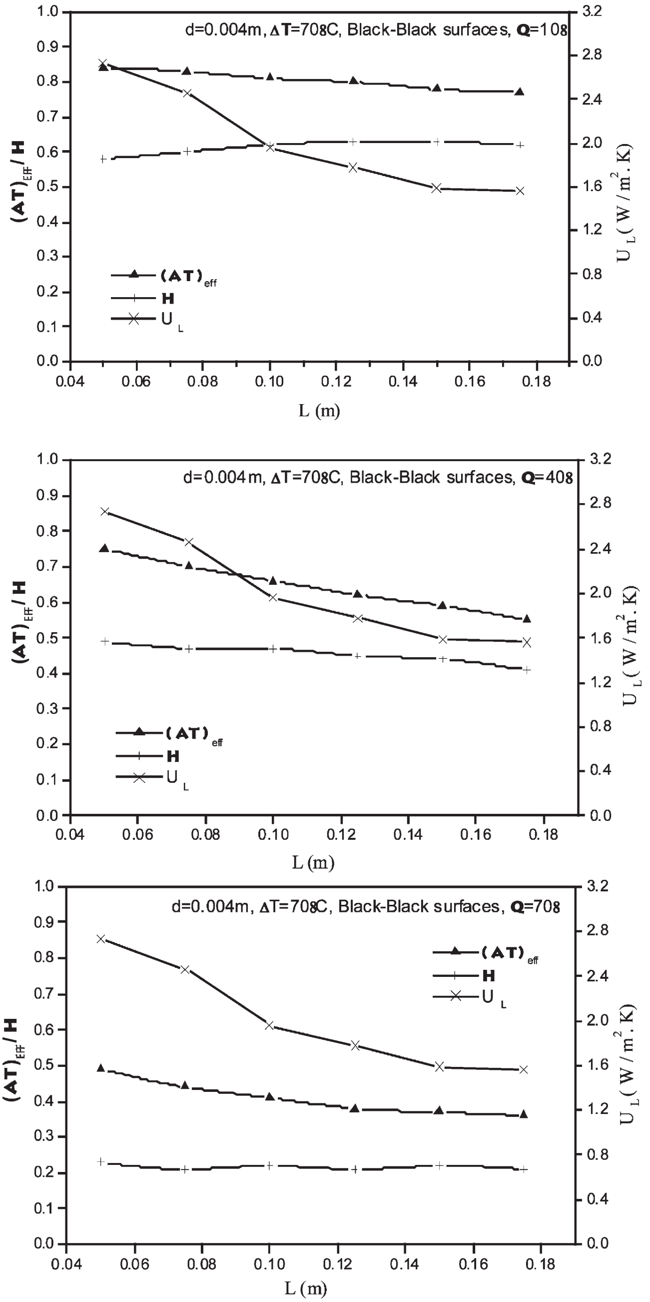


Fig. 8. $(\alpha\tau)_{eff}$, η and U_L of honeycomb panels (cell width (d) 0.004 mm; ΔT = 70 °C) placed on black absorber.

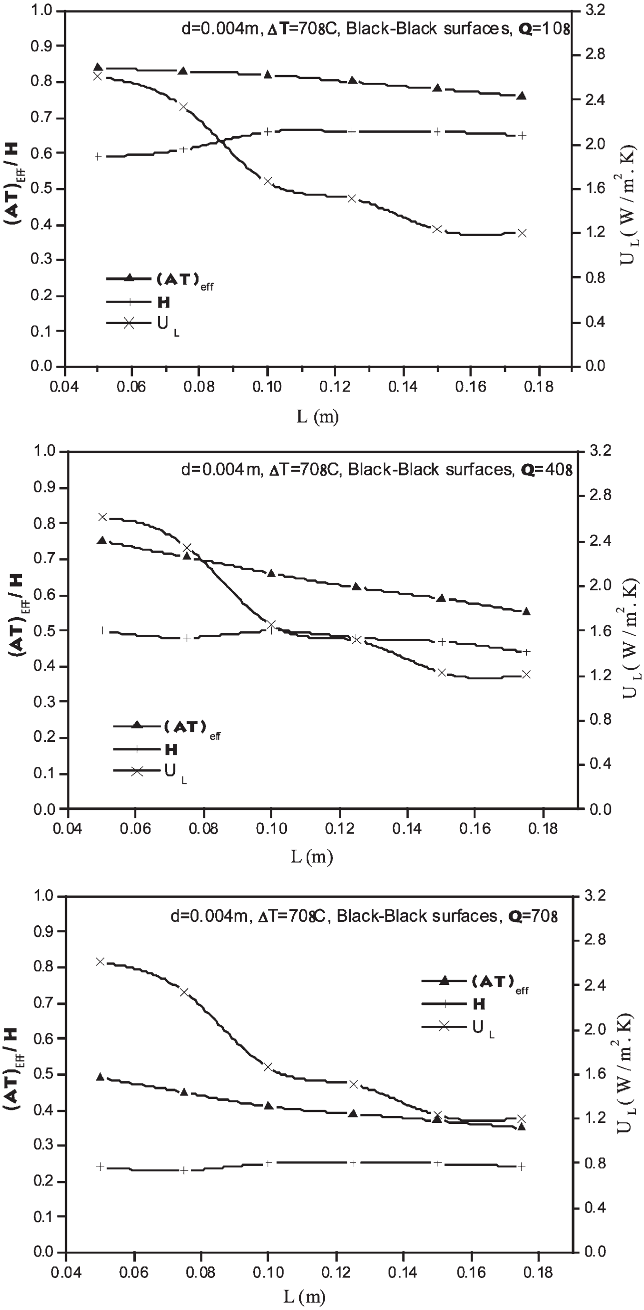


Fig. 9. $(\alpha\tau)_{\mathrm{eff}}$, η and U_L of honeycomb panels (cell width (d) 0.004 mm; $\Delta T = 70$ °C) placed on black absorber with an air gap of 10 mm.

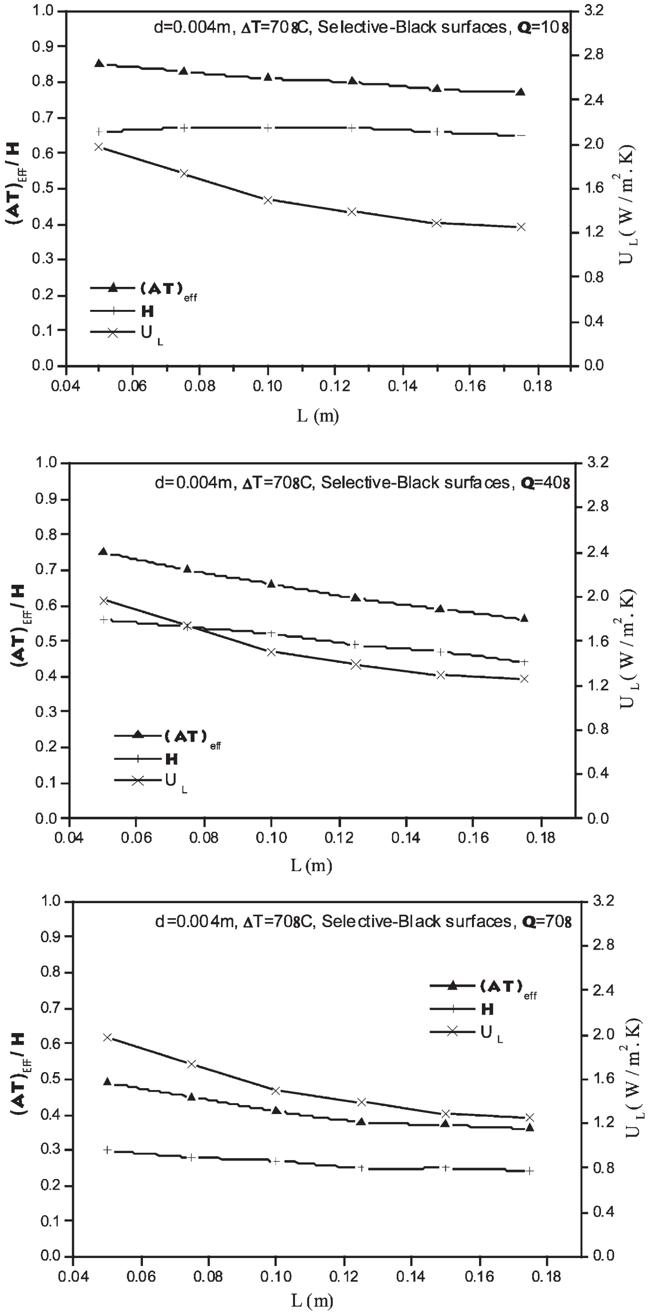


Fig. 10. $(\alpha\tau)_{eff}$, η and U_L of honeycomb panels (cell width (d) 0.004 mm; ΔT = 70 °C) placed on selective-black absorber.

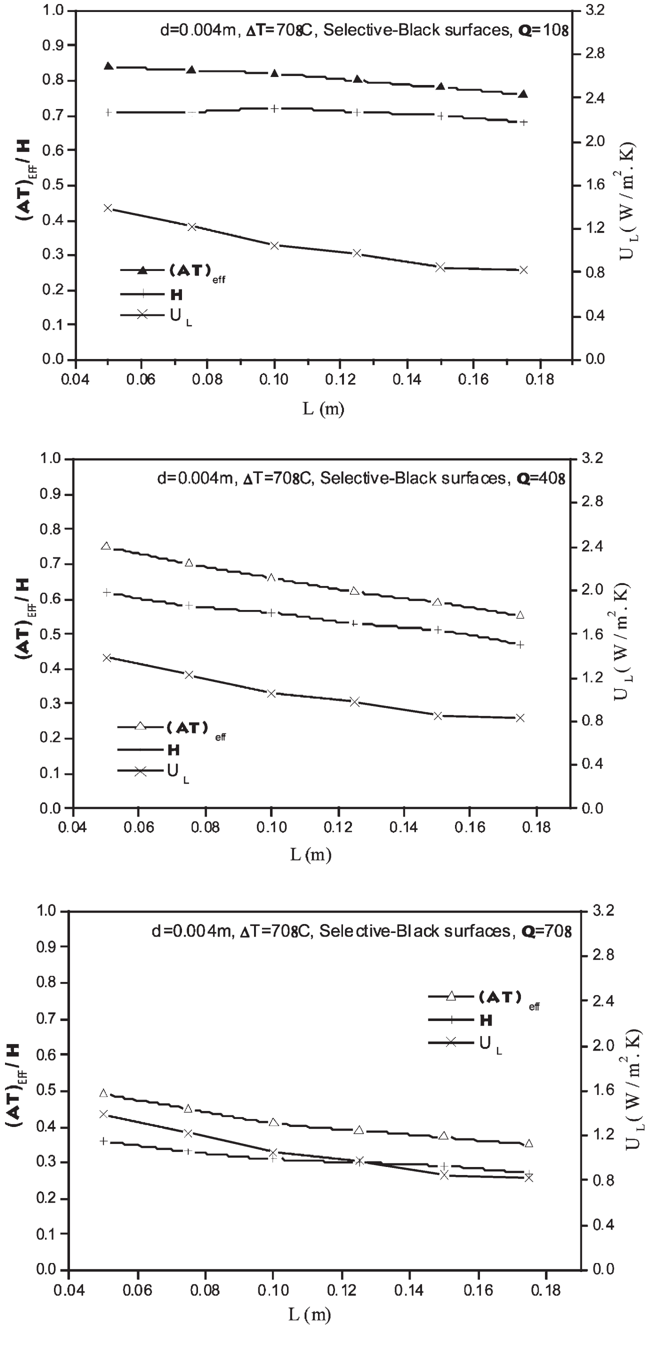


Fig. 11. $(\alpha\tau)_{\mathrm{eff}}$, η and U_{L} of honeycomb panels (cell width (d) 0.004 mm; ΔT = 70 °C) placed on selective-black absorber with an air gap of 10 mm.

Table 4
Total heat loss coefficients for three cases of bounding plates

Bounding plates	U_l (W/m^2 K)
Black–black (ε_h = 0.88, ε_c = 0.88)	2.0
Selective–black (ε_h = 0.065, ε_c = 0.88)	1.6
Selective–selective (ϵ_h = 0.065, ε_h = 0.065)	1.4

Table 5
Effect of wall emissivity on total heat loss coefficients for different bounding plate conditions

Wall emissivity (ε_w)	U_l (W/m^2 K) (L=0.10, d=0.01, T_h=306 K, T_c=298 K)					
	ε_h ε_c	0.88 0.88	0.60 0.88	0.30 0.88	0.065 0.88	0.065 0.065
0.0		0.1	1.0	2.2	4.0	5.0
0.1		1.2	1.8	2.5	3.2	3.8
0.2		1.4	1.9	2.2	2.7	3.0
0.3		1.4	1.8	2.0	2.3	2.5
0.4		1.4	2.1	1.8	2.0	2.1
0.5		1.3	1.5	1.6	1.7	1.8
0.6		1.2	1.4	1.5	1.5	1.6
0.7		1.2	1.3	1.4	1.4	1.5
0.8		1.2	1.3			1.4
0.9		1.0	1.1			1.2
1.0		0.9	1.0			1.1

Table 6
Efficiency comparison of single glazing, double glazing and MMA slab system with honeycomb cover system (I_b = 250 W/m^2, I_d = 100 W/m^2, T_p = 333 K, θ = 40 °C)

Transparent insulation thickness (m)	Efficiency			
	Single glazing	Double glazing	MMA slab	Honeycomb
0.025	0.106	0.320	0.299	0.328
0.050	0.110	0.329	0.374	0.410
0.075	0.119	0.346	0.396	0.439
0.100	0.128	0.357	0.404	0.450

7. Performance of TIM insulated solar thermal systems

Advanced glazing in flat plate solar collectors represents the most well documented application of honeycomb TIM cover systems. Rommel and Wagner [75] have exper-

Table 7
Overall heat loss coefficient (U_L) and $(\alpha\tau)_{eff}$ of various TIM cover systems

S.no.	Configuration of TIM between absorber plane and top cover	U_L (W/m^2 K)		$(\alpha\tau)_{eff}$ at $\theta = 0$
		Theoretical	Experimental	
1	Air layer	6.23	6.93	0.759
2	Glass sheet	3.73	4.63	0.658
3	Polycarbonate sheet	3.43	3.53	0.696
4	Structured sheet (6 mm)	2.63	3.43	0.565
5	Structured sheet (10 mm)	2.11	2.83	0.565
6	Cellular array (5 cm)	1.93	2.43	0.625
7	Encap. TIM (5 cm)	1.73	1.83	0.588
8	Encap. TIM (10 cm)	1.33	1.63	0.430

imentally investigated the thermal performance of flat plate solar collectors with honeycomb TIM covers and have pointed out that the TIM covers presently available (e.g. polycarbonate honeycomb TIM cover) offer good promise for application where typical working temperatures are between 40 and 80 °C and when serious material problems occur at operational temperatures above 120 °C. Therefore in the scope of the discussion on thermal performance, only low temperature solar thermal systems have been chosen such as the buildings and solar integrated-collector storage systems that use low energy materials such as water, earth, concrete and sand for collection and storage.

Solar heat gain through roof/wall/windows of buildings is a well-known means for conservation of energy used in heating indoor environments. Direct solar gain methods offer good collection efficiencies but are associated with adverse factors such as glare and radiation damage of materials inside the living space. These adverse factors are circumvented in indirect gains, which have rather low solar collection efficiencies. In recent years, TIM insulated roof/wall systems have been suggested as having the advantages of both direct and indirect gain methods. For example, Kaushika et al. [78] carried out an investigation of the dynamic thermal performance of the honeycomb roof-cover system. Periodic analysis of solar heat transfer processes in the system, comprised of an air-filled honeycomb placed on the concrete rooftop of an air-conditioned building, was carried out to investigate solar gain and assess the effectiveness of system components. An explicit expression for the heat flux entering the indoor space was derived. Results of calculations corresponding to a typical winter day at Boulder, Colorado (40°N in USA), showed that the solar gain (heat flux) of the system increases with the depth of the honeycomb. A panel at a depth 10 cm seems to be the optimum for such an application. More recently, Athienitis and Ramadan [76], have investigated the thermal performance of an outdoor test room (3 × 3×3 m) with its south facing wall transparently insulated. The transparently insulated wall system consists of an exterior single glazing, an air gap, a honeycomb-TIM slab, a second air gap, a concrete layer, an air cavity and an

interior gypsum board. A movable insulation/shading device (roller blind), may be used in the external air gap to control the thermal performance of the TIM wall. It may prevent overheating during excessive sunny periods and reduce heat losses during off-sunshine periods. For example, the blinds may be fully opened during winter days, to allow the transmission of solar radiation to the thermal mass, and closed on winter nights to reduce heat losses from the living space.

Athienitis and Ramadan [76], have developed a numerical simulation model to study the indoor temperature in the test room. The finite difference method is employed to solve the differential equation of heat conduction through the TIM insulated wall, as well as other components (walls, ceiling, floor and windows). The thermal mass (concrete layer) is discretized into five sub-layers (control volumes); more layers did not significantly improve accuracy. The finite difference approximation of the energy balance equation applied for each mode i, may be expressed as follows [76]:

$$T(\mathrm{i},t+1)=\left(\frac{\Delta t}{C_{\mathrm{i}}}\right)\cdot\left(q_{\mathrm{i}}+\sum_{\mathrm{j}}\frac{T(\mathrm{j},t)-T(\mathrm{i},t)}{R(\mathrm{i,j})}\right)+T(\mathrm{i},t)c \tag{51}$$

where j represents all nodes connected to node i, q_{i} represents all heat sources at node i, t represents the time and Δt is the time step, C_{i} is the thermal capacitance for node i and $R(\mathrm{i, j})$ represents the total thermal resistance between nodes i and j.

Numerical computations are made for mean winter conditions at Montreal (48°N in Canada). The mean outdoor temperature ($T_{0\mathrm{m}}$) is assumed to be equal to −15 °C with amplitude (ΔT) of the diurnal cycle as 5 °C. The atmospheric temperature may therefore be expressed as:

$$T=T_{0\mathrm{m}}+\Delta T\cos(\omega t-5\pi/4)$$

The transparent insulation used in numerical simulations is a square-celled honeycomb of lexan material having wall thickness 0.076 mm, with cell size 9.5 mm and aspect ratio as 5. It has U-value of 1.2 W/m^2 K. The total heat transfer coefficient across the TIM wall system is estimated to be 0.3 W/m^2 K. The indoor temperature in the test room fluctuates between 13 and 20 °C when the blind is closed at night, and it varies between 11 and 17 °C when the blind is open at night. Fig. 12 [76] shows the passive response of test room located in Montreal for seven days (starting January 21st), and with the blind closed at night. The auxiliary energy required for the room with a proportionally controlled heating system of maximum capacity of 2000 W, was evaluated. The room air temperature was permitted to fluctuate between 18 and 24 °C. An energy consumption of 14.7 MJ per day was computed with no blind control and 12.5 MJ with blind control. These results indicate significant saving of energy due to TIM walls.

The thermal performance of TIM insulated solar ICS hot water systems has been investigated theoretically as well as experimentally by Kaushika and Reddy [77]. The absorber parallel, as well as absorber perpendicular configurations of TIM devices, have been considered. The TIM cover design model considers steady state energy balance across the TIM device, which involves the solution of the fourth

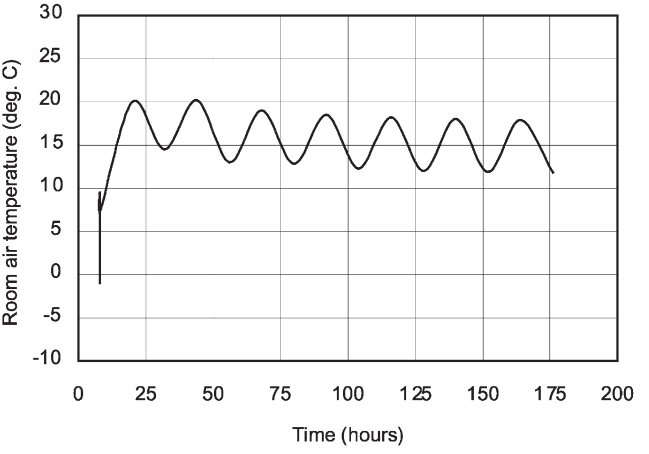


Fig. 12. Variation of indoor air temperature in the room having TIM insulated south wall with blind closed at night and located at Montreal [76].

order equation by means of an iterative process based on Newton–Raphson method. Extensive design data and trade-off for TIM cover systems are considered. Subsequently, the improvement in the performance of the ICS solar hot water system by the use of transparent insulation material in its cover system has been investigated. The field experiments on transparently insulated ICS solar water heaters have been carried out; the configuration involves the solar heating of a storage water tank, cuboid in shape and having a TIM cover system on the top surface and opaque insulation on all other sides. A simulation model is developed to evolve the optimum system design and trade-off characteristics of the TIM insulated ICS solar water heater. The model is first validated with experimental observations. Explicit simulation results on optimization of geometrical and operational parameters of the system are presented; the honeycomb depth is 5–7.5 cm and the aspect radio of 15–20 exhibit optimum performance. Compounding the honeycomb array with an air layer of 12 mm and use of a selective absorber provide the benefit of added solar gain and thermal storage. For given absorber area, the storage tank capacity enables the trade-off between system efficiency and required water temperature.

The TIM cover system characteristics significantly influence the overall system performance of the solar ICS water heater. The effectiveness of several configurations of TIM cover systems as a comparative study, has, therefore, been investigated in Fig. 13 [77]. The results of the experiments on system performance characteristics, overall heat loss coefficient and transmittance values of the cover system seem to favor the absorber perpendicular configuration over other configurations. However, the absorber-parallel configuration is simple and useful for application in passive solar water pre-heaters. The year-around thermal performance of solar water heaters with optimum design has been investigated; the simulation model, validated by experimental data, is used for this purpose. Results indicate that at New Delhi (28.6°N) the proposed system can indeed be used throughout the year for 100% of

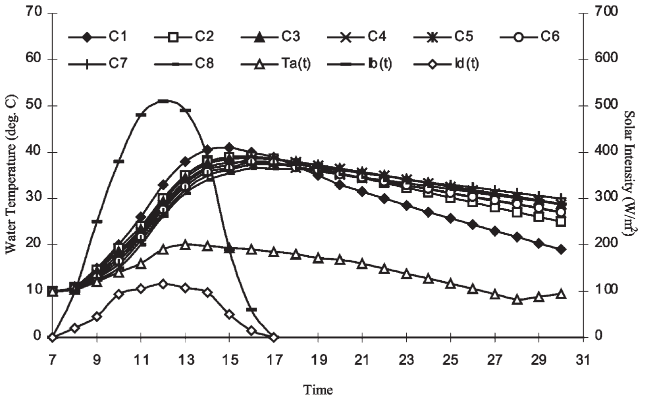


Fig. 13. Diurnal variation of water temperature in storage water heater with various TIM covers system. Location:Delhi [77].

the solar fraction for domestic water heating applications. The use of auxiliary energy has been discussed for wider applications. The demonstration of solar ICS water heaters, in accordance with user requirements, is a desirable step forward. Therefore, an research and development demonstration unit of 70 l capacity was installed at IIT Delhi to collect user data. The resulting temperature profile was found to be quite convenient for domestic water heating applications.

Field experiments with cubic water storage tanks using transparent insulation on the top surface and peripherals have also been carried out. Results suggest that incorporating transparent insulation in the solar illuminated central open could provide significant solar gain and thermal storage. The industrial water heating application of the configuration is discussed.

A TIM-insulated ground integrated-collector-storage water heating system has also been investigated for engineering design and solar thermal performance. The system consists of a network of pipes embedded in a concrete slab whose top surface is blackened and covered with the TIM device; the ground insulates the bottom. A simulation model has been developed which involves the solution of a two-dimensional transient heat conduction equation with appropriate initial and boundary conditions. An explicit finite difference scheme had been used in the numerical computations for parametric study. Emphasis is laid on such governing parameters as the depth, as well as pitch of the pipe network and collector material. A pipe network depth of 10 cm and a TIM cover made of 5 cm compound honeycomb, seems suitable for the proposed system. Solar gain (solar collection efficiency of 30–50% corresponding to temperature of 40–60 °C and the diurnal heat storage characteristics of the system are found to be of the correct order of magnitude of the solar water heating applications.

8. Summary and conclusions

This paper reviews solar transparent insulation materials in relation to their historical background, solar optical and thermal characteristics of TIM devices, their classification, fabrication, procedures, applications, availability and cost trends. TIM covers, often referred to as advanced glazing, have been shown to increase the efficiency of solar thermal conversion systems. A comparative study of TIM cover systems shows that honeycomb systems excel over other systems. TIM covers presently available (e.g. small-celled polycarbonate honeycomb TIM covers), offer good possibilities of their applications where the typical working temperatures are between 50–80 °C. However, there are many solar thermal processes with higher working temperatures in the range of 80–120 °C; these include desalination and cooling processes with adsorption and absorption cycles. Therefore, there is a need to investigate TIM for their higher working temperatures and performance, as well as low manufacturing costs. In this regard the compound honeycomb (which comprise cellular honeycomb arrays, non-convective air layer and spectrally selective covers) and parallel slat arrays should be explored. The compound honeycomb configuration holds promise for less heat loss reduction without affecting solar radiation transmittance, whereas the slat configuration enhances solar transmittance. Furthermore, the measurements of solar transmittance and total heat transport across the TIM devices are available only in assorted samples. These measurements are not yet representative of the manufacturing of devices of optimum characteristics with regard to their cost and performance.

References

[1] Tye RP. Characteristics and application of thermal insulation. In: Handbook of applied thermal design. New York: McGraw Hill; 1989.
[2] Veinberg BP, Veinberg VB. Optics in equipment for the utilization of solar energy. Moscow: State Publishing House of Defence Industry, 1959 [English translation].
[3] Francia G. A new collector of solar radiant energy: theory and experimental verification. In: Proceedings of the United Nations Conference on New Sources of Energy, Rome, 4. 1961. p. 554.
[4] Hollands KGT. Honeycomb devices in flat plate solar collectors. Solar Energy 1965;21:231.
[5] Tabor H. Honeycomb (cellular) insulation. Solar Energy 1969;25:269.
[6] Kaushika ND. Computer-aided design and fabrication of TIM from extrusion products for solar energy application. Final technical report, Indian Institute of Technology, MNES Research Scheme No. 15/1/92-ST, 1997.
[7] Edwards DK, Catton I. Prediction of heat transfer by natural convection in closed cylinders heated from below. International Journal of Heat and Mass Transfer 1969;12:23.
[8] Heitz WL, Westwater JW. Critical Rayleigh numbers of natural convection of water constrained in square cells with 4D from 0.5 to 8. Journal of Heat Transfer, ASME 1971;93(11):188.
[9] Hart J. Stability of flow in a differentially heated inclined box. Journal of Fluid Mechanics 1971;47:547.
[10] Buchberg H, Lalude OA, Edwards DK. Performance characteristics of rectangular honeycomb solar thermal convectors. Solar Energy 1971;13:193.
[11] Charters WWS, Peterson LF. Free convection suppression using honeycomb cellular materials. Solar Energy 1972;13:353.

[12] Catton I, Ayyaswany PS, Clever RM. Natural convection flow in finite rectangular slot arbitrarily oriented with respect to gravity vector. International Journal of Heat and Mass Transfer 1974;17:173.
[13] Buchberg H, Edwards DK. Design considerations for solar collectors with cylindrical glass honeycombs. In: Proceedings of International Solar Enengy Society, UCLA, USA. 1975.
[14] Cane RLD, Hollands KGT, Raithby GD, Unny TE. Free convection heat transfer across inclined honeycomb panels. Transactions of the ASME, Journal of Heat Transfer 1977;99:86.
[15] Buchberg H, Catton I, Edwards DK. Natural convection in enclosed spaces: a review of application to solar energy collection. Transactions of the ASME, Journal of Heat transfer 1976;98:182.
[16] Koutsoheras W, Charters WW. Natural convection phenomenon in inclined cells with finite side walls—a numerical solution. Solar Energy 1977;19:433.
[17] Smart DR, Hollands KGT, Raithby GD. Free convection heat transfer across rectangular celled diathermanous honeycombs. Transactions of the ASME, Journal of Heat Transfer 1980;102:75.
[18] Sharma MS, Kaushika ND. Design and performance characteristics of honeycomb solar pond. Energy Conversion and Management 1987;32:345.
[19] Guthrie KI, Charters WWS. An evaluation of transverse slatted flat plate collector. Solar Energy 1982;28:89.
[20] Kaushika ND, Padmapriya R, Singh TP. Convection theory of honeycomb and slat devices for solar energy applications. Energy Resource and Technology 1992;2:125.
[21] Lalude O, Buchberg H. Design and application of honeycomb porous-bed solar-air heaters. Solar Energy 1971;12:223.
[22] Hollands KGT, Raithby GD, Russel FB, Wilkinson RG. Coupled radiative and conductive heat transfer across honeycomb panels and through single cells. International Journal of Heat Transfer 1984;27:2119.
[23] Charters WWS, Guthrie KI. Experimental evaluation of slatted convection suppression devices. In: Solar World Forum, 1. Oxford: Pergmon Press; 1982. p. 181.
[24] Hollands KGT, Marshall KN, Wedel RK. An approximate equation for predicting the solar transmittance of transparent honeycombs. Solar Energy 1978;21:231.
[25] Symons JG. The solar transmittance of some convection suppression devices for solar energy applications: an experimental study. Transactions of the ASME, Journal of Solar Energy Engineering 1982;104:251.
[26] Symons JG. Calculation of the transmittance–absorptance product for flat-plate collectors with convection suppression devices. Solar Energy 1984;33:637.
[27] Lin EIH. A saltless solar pond. Proc Int Solar Energy Society (American Section of ISES) 1982;225.
[28] Goetzberger A, Schmidt J, Wittwer V. Transparent insulation system for passive solar energy utilization in buildings. Solar Energy 1984;2:289.
[29] Hollands KGT, Iynkaran K. Proposal for a compound honeycomb collector. Solar Energy 1985;34:309.
[30] Ortabassi U, Dyksterhuis FH, Kaushika ND. Honeycomb stabilized saltless solar pond. Solar Energy 1983;31:229.
[31] Kaushika ND, Banerjee MB, Katti Y. Honeycomb solar pond collector storage system. Energy 1983;8:883.
[32] Schaefer R, Lowrey P. The optimum design of honeycomb solar ponds and a comparison with salt gradient solar ponds. Solar Energy 1992;48:69.
[33] Koushika ND, Banerjee MB. Honeycomb solar pond: evaluation of applications. In: Solar World Congress, Perth, Australia. 1983. p. 246.
[34] Goetzberger A, Rommel M. Prospects for integrated storage collector system in Europe. Solar Energy 1987;39:211.
[35] Kaushika ND, Ray RA, Padmapriya R. A honeycomb solar collector and storage system. Energy Conversion and Management 1990;30(2):127.
[36] Avanti P, Arulanantham M, Kaushika ND. Solar thermal analysis of ground integrated collector/storage system with transparent insulation. Applied Thermal Engineering 1996;16(11):863.
[37] Rubin M, Lambert CM. Transparent silica aero gel for window insulation. Solar Energy Material 1983;7:393.

[38] Kaushika ND, Sharma MS, Sanjay K. Honeycomb roof cover system for passive solar space heating. Energy Conversion and Management 1987;27:98.
[39] Gordon JM. Low heat loss double-glazed windows. Energy 1987;12:1333.
[40] Goetzberger A, Dengler J, Rommel M, Gottsche J, Wittwer V. A transparently insulated bifacially irradiated solar flat plane collector. Solar Energy 1992;49:403.
[41] Chevalier B, Hutchins MG, Maccari A, Olive H, Oversloot H, Platzer W et al. Solar energy transmittance of translucent samples: a comparison between large and small integrating sphere measurements. Solar Energy Materials and Solar Cells 1998;54:197.
[42] Fricke J. Aerogels. Scientifc American 1988;:92.
[43] Platzer W, Wittwer V. Transparent insulation materials. In: Granqvist CG, editor. Material science for solar energy conversion systems. Oxford: Pergamon press; 1991.
[44] Lee D, Stevens PC, Zeng SQ, Hunt AJ. Thermal characterization of carbon opacified aerogels. Journal of non-crystalline Solid 1996;186:285.
[45] Tajiri K, Nishio T, Tanemura S. Temperature dependence of thermal conductivity of advanced insulators. In: ISES 1999 Solar World Congress, Jerusalem, Israel, July 4–9, I. 1999. p. 482.
[46] Cobble MH. Irradiation into transparent solids and the thermal trap effect. Journal of Franklin Institute 1964;278:383.
[47] Cobble MH, Fang PC, Lumsadine E. Verification of the theory of the thermal trap. Journal of Franklin Institute 1966;282:102.
[48] Hakim G. A new heat reflective polycarbonate sheet with spectral selectivity. In: ISES 1999 Solar World Congress, Jerusalem, Israel, July 4–9, I. 1999. p. 461.
[49] Hollands KGT. Advanced non-concentrating solar collectors. In: Dixon AE, Leslie JD, editors. Solar energy conversion. An introductory course. Oxford: Pergamon Press; 1979.
[50] Arnold JN, Catton I, Edwards I. Experimental investigation of natural convection in inclined rectangular regions of different aspect ratios. Transactions of the AMSE Journal of Heat Transfer 1976;98:67.
[51] Platzer WJ. Calculation procedure for collectors with a honeycomb cover of rectangular cross section. Solar Energy 1992;48:381.
[52] Platzer WJ. Directional-hemispherical solar transmittance data for plastic type honeycomb structures. Solar Energy 1992;49:359.
[53] Kaushika ND, Padmapriya R. Solar transmittance of honeycomb and parallel slat arrays. Energy Conversion and Management 1991;32:345.
[54] Hollands KGT. Designing honeycombs for minimum material and maximum transmission. In: Jesch LF, editor. Proceedings of 2nd International Workshop on Transparent insulation, Freiburg, Germany, March 24–25. Transparent insulation-2. Birmingham, UK: Franklin Company Consultants Ltd.; 1988. p. 40.
[55] Symons JG, Christie EA, Peck MA. Integrating sphere for solar transmittance measurement of planar and non-planar samples. Applied Optics 1982;21(15):2827.
[56] Platzer WJ. Total heat transparent data for plastic honeycomb-type structures. Solar Energy 1992;49:351.
[57] Rommel M, Wagner A. Application of transparent insulation materials in improved flat-plate collectors and integrated collector storages. Solar Energy 1992;49(5):371.
[58] Sabberwal SP, Prakash J, Seth A. Enhancement of solar gains through a roof using a thermal trap. Energy Conversion and Management 1985;25:249.
[59] Prakash J, Carnevale E. Use of thermal trap material for space heating of non-air conditioned buildings. Energy Conversion and Management 1987;27:205.
[60] Prakash J, Carnevale E. Performance prediction of two models of solar water heaters using a thermal trap. Energy Conversion and Management 1987;27:21.
[61] Prakash J, Kaushika SC, Kumar R, Garg HP. Performance prediction for a triangular built-in storage-type solar water heater with transparent insulation. Energy 1994;19:869.
[62] San Martin RL, Fjeld GJ. Experimental performance of three solar collectors. Solar Energy 1975;17:345.
[63] Kaushika ND, Arulanantham M. Radiative heat transfer across transparent honeycomb insulation materials. International Journal of Heat and Mass Transfer 1995;22(5):751.

[64] Arulananatham M, Reddy KS, Kaushika ND. Solar gain characteristics of absorber-parallel transparent insulation material. Energy Conversion and Management 1998;36(15):1519.
[65] Brandemuehl MJ, Beckman WA. Transmission of diffuse radiation through CPC and flat plate collectors glazing. Solar Energy 1980;24:511.
[66] Arulanantham M, Kaushika ND. Global radiation transmittance of transparent insulation materials. Solar Energy 1994;53:323.
[67] Kaushika ND, Arulanantham M. Transmittance–absorptance product of solar glazing with transparent insulation materials. Solar Energy Materials and Solar Cells 1996;44:383.
[68] Arulanantham M, Kaushika ND. Coupled radiative and conductive thermal transfers across transparent honeycomb insulation materials. Applied Thermal Engineering 1996;16(3):209.
[69] Duffie JA, Beckman WA. Solar engineering of thermal process., 2nd ed. New York: John Wiley & Sons, Inc., 1991.
[70] James ML, Smith GM, Wolford JC. Applied numerical methods for digital computation. New York: IEP, A Dun-Donnelley publishers, 1977.
[71] Feland JR, Edwards DK. Solar and infrared radiation properties of parallel plate honeycomb. Energy 1978;2:275.
[72] Platzer WJ. Solar transmittance of transparent insulation materials. Solar Energy Materials 1987;16:275.
[73] Kaushika ND, Padmapriya R, Arulanantham M, Sharma PK. Transparent insulation characteristics of honeycomb and slat arrays. Energy 1994;19:1037.
[74] Reddy KS, Kaushika ND. Comparative study of TIM cover systems for integrated-collector-storage solar water heaters. Solar Energy Materials and Solar Cells 1999;58:431.
[75] Rommel M, Wagner A. Application of transparent insulation materials in improved flat-plate collectors and integrated collector storage system. Solar Energy 1992;49:371.
[76] Athientis AK, Ramadan H. Numerical model of a building with transparent insulation. In: ISES 1999 Solar World Congress, Jerusalem, Israel, July 4–9, II. 1999. p. 10.
[77] Koushika ND, Reddy KS. Performance of transparently insulated solar passive hot water systems. In: ISES 1999 Solar World Congress, Jerusalem, Israel, July 4–9, III. 1999. p. 203.
[78] Kaushika ND, Sharma PK, Padmapriya R. Solar thermal analysis of honeycomb roof cover system for energy conservation in an air conditioned building. Energy and Building 1992;18:45–9.